Scaling method for fast Monte Carlo simulation of diffuse reflectance spectra from multilayered turbid media

Quan Liu and Nirmala Ramanujam

Department of Biomedical Engineering, Duke University, 136 Hudson Hall, Box 90281, Durham, North Carolina 27708-0281, USA

Received September 13, 2006; revised November 20, 2006; accepted November 22, 2006; posted December 8, 2006 (Doc. ID 74956); published March 14, 2007

A scaling Monte Carlo method has been developed to calculate diffuse reflectance from multilayered media with a wide range of optical properties in the ultraviolet–visible wavelength range. This multilayered scaling method employs the photon trajectory information generated from a single baseline Monte Carlo simulation of a homogeneous medium to scale the exit distance and exit weight of photons for a new set of optical properties in the multilayered medium. The scaling method is particularly suited to simulating diffuse reflectance spectra or creating a Monte Carlo database to extract optical properties of layered media, both of which are demonstrated in this paper. Particularly, it was found that the root-mean-square error (RMSE) between scaled diffuse reflectance, for which the anisotropy factor and refractive index in the baseline simulation were, respectively, 0.9 and 1.338, and independently simulated diffuse reflectance was less than or equal to 5% for source–detector separations from 200 to 1500 μm when the anisotropy factor of the top layer in a two-layered epithelial tissue model was varied from 0.8 to 0.99; in contrast, the RMSE was always less than 5% for all separations (from 0 to 1500 μm) when the anisotropy factor of the bottom layer was varied from 0.7 to 0.99. When the refractive index of either layer in the two-layered tissue model was varied from 1.3 to 1.4, the RMSE was less than 10%. The scaling method can reduce computation time by more than 2 orders of magnitude compared with independent Monte Carlo simulations.

OCIS codes: 300.6540, 300.6550, 290.1350, 290.4210, 290.7050, 170.3660.

1. INTRODUCTION

Ultraviolet–visible (UV-VIS) diffuse reflectance spectroscopy has been explored to detect precancers and cancers in a variety of epithelial tissues.[1–5] This nondestructive technique has several attributes. First, diffuse reflectance spectra contain a wealth of biochemical and structural information related to disease progression.[6–9] Moreover, broadband light sources, sensitive detectors, and compact fiber-optic probes enable rapid and remote measurements of diffuse reflectance from tissue surfaces and endoscopically accessible organ sites. In such applications, an accurate model of light transport is essential to quantitatively extract optical properties from measured diffuse reflectance spectra. Diffusion theory and the modified versions of this analytical model have been used to extract optical properties and relevant biochemical and structural information from diffuse reflectance measurements previously.[3–5,10] However, diffusion theory is not valid to describe light propagation at small source–detector separations[11] and for the case where absorption and scattering are comparable, such as diffuse reflectance measurements in the UV-VIS spectral region. In these situations, the Monte Carlo method provides a flexible tool to model light transport in turbid media. In addition, the capability of Monte Carlo modeling to simulate complex tissue structures and fiber-optic geometries has made it very attractive as a model of light transport. However, the main drawback of the Monte Carlo method is the requirement of intensive computation to achieve results with desirable variance, which makes it extremely time consuming compared with analytical models such as diffusion theory.

There has been a lot of work previously to improve the efficiency of the Monte Carlo method for modeling light transport in turbid media. Several publications have demonstrated the use of improved Monte Carlo methods, or simply Monte Carlo databases created beforehand with conventional Monte Carlo modeling, to estimate the optical properties of the tissue from given diffuse reflectance data in the spatial,[12,13] time,[14] or frequency domains[3,15] and/or as a function of wavelength.[2] The methods proposed to increase the efficiency of Monte Carlo modeling can be broadly separated into two groups: the methods accelerating a single Monte Carlo simulation[16–18] and the methods taking advantage of information generated by a small set of Monte Carlo baseline simulations for a wide range of optical properties.[14,15,19–23]

The first set of methods[16–18] can accelerate a single Monte Carlo simulation to achieve desirable variance in simulated results. For example, the geometry-splitting technique can increase the fraction of useful photons for a specific fiber-optic probe geometry, thus reducing the total number of incident photons needed to minimize the variance of simulated diffuse reflectance.[16,17] Tinet *et al.*[18] proposed a semianalytical Monte Carlo method for time-resolved light propagation. Each random-walk step of a photon contributes deterministically to a detector area, thus dramatically improving the variance of detected sig-

nals especially when the goal is to simulate rarely occurring events.

The second set of methods[14,15,19–23] takes the information collected from a single baseline simulation or a small set of baseline simulations and uses them to generate diffuse reflectance or transmittance for a wide range of optical properties. For example, the reciprocity theorem has been employed to reduce the number of Monte Carlo simulations for fluorescence propagation in layered media.[23] The perturbation Monte Carlo method records the trajectory information for each individual detected photon in a baseline simulation and adjusts the exit weight of the photons for small changes of optical properties in layered media[15] or for the perturbation of small heterogeneities present in a homogeneous medium[22] according to proper differential operators. However, the accuracy of the perturbation method is sensitive to changes in the scattering coefficient,[15,22] thus limiting the applicable range of the data generated from a single baseline simulation. The scaling method is another powerful approach that requires photon trajectory information from a baseline simulation. Battistelli *et al.*[19] proposed two scaling relations for calculation of transmittance in a Monte Carlo simulation. Graaff *et al.*[20] took advantage of the fact that the step sizes of random walk in a Monte Carlo simulation are linearly related to the inverse of the transport coefficient (sum of absorption and scattering coefficients) and developed two very useful scaling relations, one of which relates the exit distance of a photon to the transport coefficient of a homogeneous medium and the other relates the exit weight to the albedo. Kienle and Patterson[14] created a Monte Carlo database for the estimation of optical properties of a homogeneous medium from given time-resolved reflectance by using the relations proposed by Graaff *et al.*[20] to account for the change in the scattering coefficient and using Beer's law to account for the absorption coefficient. Palmer and Ramanujam[21] developed a scaling Monte Carlo method to extract optical properties from diffuse reflectance spectra of a homogeneous medium in the UV-VIS spectral region. Again, the scaling approach by Graaff *et al.*[20] was used such that only a single Monte Carlo simulation was needed for a particular fiber-optic probe geometry. Unfortunately, none of these studies addresses the need for a method that can implement fast Monte Carlo simulations of diffuse reflectance from multilayered turbid media.

Our group has extended the capabilities of the scalable Monte Carlo model developed by Palmer and Ramanujam[21] to sequentially estimate the optical properties of a two-layered squamous epithelial tissue model.[16] In the second step of this sequential estimation method, a database that contains diffuse reflectance data simulated from the two-layered tissue model for a wide range of optical properties was required prior to the inversion process to estimate the optical properties of the bottom layer (assuming that the optical properties of the top layer have been obtained in the first step). To reduce the number of required independent simulations, a strategy called white Monte Carlo simulation was used.[14,23] Several Monte Carlo simulations were run with zero absorption and various scattering coefficients, and the path lengths of detected photons were recorded. The effect of absorption was incorporated postsimulation according to Beer's law. Although this strategy reduced the total number of simulations by roughly 3 orders of magnitude, it still required a significant number of independent simulations (a total of 819 simulations, each with 10^6 incident photons), which took about four weeks to complete on a cluster of Sun UNIX computers equipped with the CONDOR distributed computing software.[24]

This paper describes a multilayered scaling method that enables implementation of fast Monte Carlo simulations of diffuse reflectance from multilayered turbid media. This method requires photon trajectory information provided by only a single baseline simulation, from which the diffuse reflectance can be computed for a wide range of optical properties in a multilayered turbid medium. A convolution scheme is also incorporated to calculate diffuse reflectance for specific fiber-optic probe geometries. The multilayered scaling approach for computing diffuse reflectance was demonstrated for a two-layered and a three-layered epithelial tissue model and validated by quantitatively comparing scaled results with diffuse reflectance obtained from independent Monte Carlo simulations. In addition, a diffuse reflectance spectrum simulated from the two-layered tissue model for a source–detector separation of 1500 μm was used as the input to the sequential estimation method[16] described previously to evaluate the errors in retrieving the optical properties of the bottom layer and the thickness of the top layer of the tissue model where a Monte Carlo database created by the multilayered scaling method was employed in the inversion (assuming that the optical properties of the top layer are known).

2. METHODS

A. Principle of the Multilayered Scaling Method

In principle, the multilayered scaling method is similar to the scaling method for a homogeneous medium as described by Graaff *et al.*[20] For the purpose of comparison, Fig. 1(a) illustrates the scaling method as applied to a homogeneous medium. The solid lines with arrows represent the trajectory of a photon in a baseline medium, and the dashed lines with arrows are the scaled trajectory for a new medium where the transport coefficient (μ_t) is half of the baseline value. When μ_t decreases by one half, the mean free path of the photon, which is the reciprocal of μ_t, increases by a factor of 2. Subsequently, the exit location of the photon after scaling is displaced from the incident location by a factor of 2 relative to the original exit location if every step of the random walk is sampled with exactly the same random numbers as in the baseline simulation.

The above procedure can be mathematically formulated as follows. Some key notations are defined first. The transport coefficient denoted by μ_t is the sum of the absorption (μ_a) and scattering (μ_s) coefficients. The albedo is denoted by α, and $\alpha=\mu_s/\mu_t$. Assume the transport coefficient in the baseline medium is μ_{t0} and the albedo is α_0. The number of collisions that a photon experiences before exit is N, and the photon escapes from the top surface of the medium at a distance of r_0 from the incident location (which will be called the exit distance from now on). Then

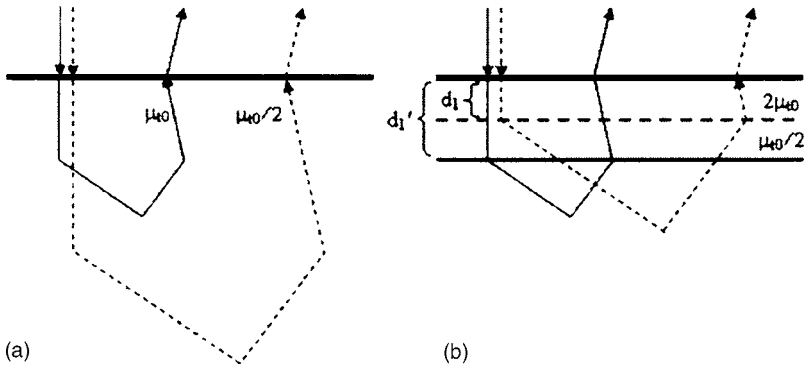

Fig. 1. Principle of the scaling method as applied in (a) a homogeneous medium and (b) a two-layered medium. In both (a) and (b), the horizontal bold line is the air–medium interface, the solid lines with arrows represent the trajectory of a photon in a baseline medium, and the dashed lines with arrows represent the scaled trajectory of the same photon in a new medium with a different set of optical properties. The incident locations of the two trajectories were supposed to overlap, but they were purposefully shifted away from each other in the above figures for better differentiation. The baseline transport coefficient (μ_t) is μ_{t0} in both (a) and (b). For homogeneous scaling in (a), it is assumed that the new μ_t is half of μ_{t0}. For the layered scaling in (b), it is assumed that the μ_t of the top layer is twice μ_{t0} and the μ_t of the bottom layer is half of μ_{t0}. In (b), the horizontal dashed line in the middle stands for the layer interface in the two-layered medium, while the horizontal solid line in the bottom represents the corresponding location of the layer interface in the baseline medium as if the baseline medium were two-layered with a pseudolayer interface.

the photon weight upon exit is $w_0=\alpha_0^N$. For a new set of optical properties where the transport coefficient is μ_t and the albedo is α, the scaled exit distance is $r=r_0\times\mu_{t0}/\mu_t$, and the exit weight is $w=\alpha^N=w_0\times(\alpha/\alpha_0)^N$.

Figure 1(b) illustrates the scaling method as applied to a two-layered medium. Again, the solid lines with arrows are the trajectory of a photon in a baseline homogeneous medium with a transport coefficient of μ_{t0}, and the dashed lines are the scaled trajectories in a two-layered medium. In this example, the top layer μ_t is twice μ_{t0}, the bottom layer μ_t is half of μ_{t0}, and the top-layer thickness is d_1 (the dashed horizontal line indicates the layer interface between the top and the bottom layers in the two-layered medium). The first step in the scaling process is to find the corresponding location of the layer interface in the baseline medium. Because the top layer μ_t is twice μ_{t0}, the mean free path in the top layer is half of that in the baseline medium. Therefore the top-layer thickness should be doubled to obtain the corresponding location of the layer interface in the baseline medium, i.e., $d_1'=2d_1$. Thus, the baseline medium can be viewed as a pseudo-two-layered medium with a pseudolayer interface at depth $d_1'=2d_1$. The random-walk steps of the photon in the baseline medium can then be separated into two groups according to their location relative to the pseudolayer interface in the baseline medium. Any steps that are within the pseudo top layer (depth smaller than d_1') are scaled according to the optical properties of the top layer in the two-layered medium. Similarly, the steps that are within the pseudo bottom layer (depth larger than d_1') in the baseline medium are scaled according to the optical properties of the bottom layer in the two-layered medium. In this specific situation, all photon steps in the top layer are cut short by half, and all photon steps in the bottom layer are stretched by a factor of 2. The exit distance of the photon is the vector sum of the scaled steps in the horizontal dimension (in the plane parallel to the medium top surface where diffuse reflectance is measured) as shown in Fig. 1(b).

Similar to the previous procedure for homogeneous scaling, the above procedure for multilayered scaling can be mathematically formulated as follows. Assume the transport coefficient in the baseline medium is μ_{t0}, the albedo is α_0, and the exit weight of a specific photon is w_0. It is further assumed that the multilayered medium has a total of n layers and the transport coefficient of the first layer in the medium is μ_{t1}, that of the second layer is $\mu_{t2},\ldots$, and that of the nth layer is μ_{tn}. Similarly, the albedo for each layer is $\alpha_1,\alpha_2,\ldots,\alpha_n$, and the thickness of each layer is $d_1,d_2,\ldots,d_n$. For every photon that exits from the top surface of the baseline medium, do the following:

I. Determine the corresponding locations of all the layer interfaces in the baseline medium. This step needs to be done only once for all photons. The thicknesses of these pseudolayers can be obtained by the following scaling operations:

$$d_1'=d_1\times\mu_{t1}/\mu_{t0},$$

$$d_2'=d_2\times\mu_{t2}/\mu_{t0},$$

$$\cdots$$

$$d_n'=d_n\times\mu_{tn}/\mu_{t0}.$$

II. Determine the number of collisions that the photon experienced, N_i, and the horizontal offset that the photon traveled, r_i, in each pseudolayer before exit based on the trajectory information from the baseline simulation ($i=1,2,\ldots n$).

III. Scale the horizontal offset in each pseudolayer according to the transport coefficient of the corresponding real layer, and take the vector sum of the horizontal offsets in all layers, which yields the scaled exit distance

$$r=\sum_{i=1}^{n}(r_i\times\mu_{t0}/\mu_{ti}),$$

where r_i is the horizontal offset recorded in the ith pseudolayer.

IV. Calculate the weight change in each pseudolayer according to the albedo of each real layer and the number of collisions in each pseudolayer, and take the product of all the weight change terms, which yields the scaled exit weight:

$$w = \prod_{i=1}^{n} (\alpha_i/\alpha_0)^{N_i} \times w_0,$$

where N_i is the number of collisions in each pseudolayer and w_0 is the exit weight in the baseline simulation.

It should be pointed out that the horizontal offsets refer to either the x or the y dimension in a Cartesian coordinate system. To obtain the radial offsets, the offsets in the x and y dimensions should be scaled separately and then recombined in the end. Therefore, both x and y offsets are needed for scaling in a three-dimensional light transport model. In addition, when one random-walk step crosses two or more pseudolayers, the horizontal offset corresponding to this step should be distributed to all relevant layers according to the path length of the photon in each pseudolayer. For simplicity, it is assumed that the baseline homogeneous medium and the bottom layer of the multilayered medium are semi-infinite in the axial dimension and infinite in the lateral dimension.

B. Monte Carlo Baseline Simulation for Multilayered Scaling and Scaling Operation

A three-dimensional, weighted-photon Monte Carlo code written with standard American National Standards Institute (ANSI) C programming language[25,26] was modified to create a photon trajectory database for scaling. A single simulation was run for a homogeneous baseline medium, in which $\mu_a = 0\ \text{cm}^{-1}$, $\mu_s = 100\ \text{cm}^{-1}$, and the anisotropy factor $g = 0.9$. The Henyey–Greenstein (HG) phase function was used for sampling scattering angles in the simulation. The refractive index of the medium above the baseline medium, the refractive index of the baseline medium, and the refractive index of the medium below the baseline medium were set at 1.462, 1.338, and 1.338, respectively. These two values represent the refractive indices of glass and water at 500 nm.[27,28] The thickness of the medium was set at 5 cm to simulate a semi-infinite medium. A total of 4×10^6 photons was launched at the origin of a Cartesian coordinate system to obtain the impulse response of the baseline medium in diffuse reflectance. The Cartesian coordinate system was set up such that the axial dimension, which is perpendicular to the top surface of the baseline medium, corresponds to the z axis, and the x–y plane is parallel to the top surface of the baseline medium. The angular profile of incident photons (relative to the z axis) followed a Gaussian distribution with a cutoff angle defined by a numerical aperture (NA) of 0.22 to simulate an optical fiber. The axial dimension of the baseline medium was empirically divided into 51 depth intervals with variable interval widths to record photon trajectory information. The interval width was progressively increased with depth because the likelihood of photon visitations decreases with depth. The actual depth interval width was assigned as follows: 50 μm for depths from 0 to 0.1 cm, 100 μm for depths from 0.105 to 0.475 cm, 350 μm for a depth of 0.485 cm, 500 μm for depths from 0.52 to 0.92 cm, 800 μm for a depth of 0.97 cm, and 1000 μm for depths from 1.05 to 1.85 cm. All depths beyond 1.95 cm are assigned to the last depth interval. When a photon exits at an angle relative to the z axis smaller than the cutoff angle defined by an NA of 0.22, the relevant trajectory information of this photon, which includes the exit weight, the x and y offsets, and the number of collisions of the photon within each depth interval, is stored in a numerical array. Approximately 1.2×10^5 photons were detected on the top surface of the baseline medium, and a memory space of 160 MBytes was needed to store the trajectory data.

Because the depth intervals have finite width, the pseudolayer interfaces in the baseline medium, whose locations are obtained by scaling the depth of the layer interfaces in the multilayered medium, can be located within a depth interval rather than exactly at a boundary between two adjacent intervals. In this case, all the x and y offsets as well as the number of collisions corresponding to this interval need to be distributed between the two relevant pseudolayers. The contribution to each layer is linearly proportional to the fraction of the interval width within that layer.

After the impulse response of the multilayered medium in diffuse reflectance is obtained by using the scaling method, the diffuse reflectance for a specific fiber-optic source–detector geometry can be calculated by convolving the impulse response with the beam profile.[21,25] All the scaling operations were coded and run in MATLAB 6 (MathWorks, Incorporated, Natick, Massachusetts).

C. Theoretical Tissue Models and Specific Fiber-Optic Probe Geometries

The scaling method was tested on a two-layered model and a three-layered model of human squamous epithelial tissue. The corresponding diffuse reflectance from the two epithelial tissue models was also independently simulated with a Monte Carlo code[26] for comparison with the scaled diffuse reflectance. The HG function was used in the independent simulations except when the effect of the phase function was studied (Fig. 7 and Tables 4 and 8 below).

Figure 2 shows the schematics of the two epithelial tissue models. In Fig. 2(a), the top-layer thickness d_1 is 500 μm, and the bottom-layer thickness d_2 is 5 cm to simulate a semi-infinite medium. In Fig. 2(b), the top-layer thickness d_3 is varied from 50 to 250 and to 450 μm while the sum (d_1) of the top-layer and the middle-layer thicknesses is fixed at 500 μm. The middle layer in the three-layered model is intended to simulate a sublayer of neoplastic cells in the epithelial layer.

The optical properties of the tissue model are shown in Fig. 3(a) for the top layer, in Fig. 3(b) for the bottom layer, and in Fig. 3(c) for the middle layer. The optical properties of the top and bottom layers are exactly the same as those in a previous publication[16] from our group to facilitate comparison of the accuracy of optical property estimation later using the multilayered scaling method with the accuracy using the previously developed sequential estimation method.[16] The ranges of optical properties were chosen to represent those of human cervical tissue.[29]

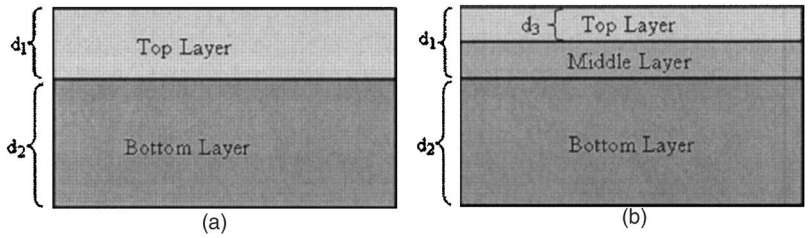

Fig. 2. Schematics of two-layered and three-layered epithelial tissue models for testing the accuracy of the multilayered scaling method. The optical properties of the top layer are shown in Fig. 3(a), the optical properties of the bottom layer are shown in Fig. 3(b), and the optical properties of the middle layer are shown in Fig. 3(c). It should be noted that the thicknesses of the top layer and the middle layer in (b) add up to the thickness of the top layer in (a).

The absorption coefficients of the middle layer are identical to those of the top layer, while the scattering coefficients of the middle layer are twice those of the top layer to approximate a precancerous layer.[7] Absorption and scattering were assumed to be contributed, respectively, by Nigrosin at known concentrations and polystyrene spheres with a diameter of 1.053 μm and a volume concentration of 0.256%. Mie theory[30] was used to calculate the scattering properties of the polystyrene spheres. The refractive indices of the spheres and water were assumed to be 1.6 and 1.3352, respectively, in the calculation.

The refractive index of the medium above the tissue models, the refractive index of the tissue models, and the refractive index of the medium below the tissue models were 1.462, 1.338 and 1.338, respectively. The value of g was 0.9 unless specified otherwise. These parameters are maintained equal to those in the baseline simulation for scaling as described in the previous subsection to achieve "ideal conditions" for evaluation of scaled reflectance in Subsection 3.A. They will be varied to examine the valid range of scaled reflectance in Subsection 3.B. The diameter of both source and detector fibers was 200 μm, and the NA was fixed at 0.22 for these simulations. The center-to-center distance between the source and the detector fibers was varied from 0 to 2000 μm with a uniform increment of 200 μm.

3. RESULTS

A. Accuracy of Scaled Reflectance Relative to Independently Simulated Reflectance under Ideal Conditions

To test the accuracy of scaled diffuse reflectance under ideal conditions, the reflectance was independently simulated on the original two-layered epithelial model, in which the same anisotropy factor, refractive indices, and phase function as used in the baseline simulation were employed. Each independent simulation was run six times. The percent deviation between scaled and simulated results at each individual wavelength was calculated as follows to quantify the accuracy of the scaled results and is shown in Figs. 4 and 5:

$$\text{Percent Deviation} = \frac{\text{Scaled-Simulated}}{\text{Simulated}} \times 100, \quad (1)$$

where "Scaled" represents the scaled reflectance value and "Simulated" represents the mean of simulated reflec-

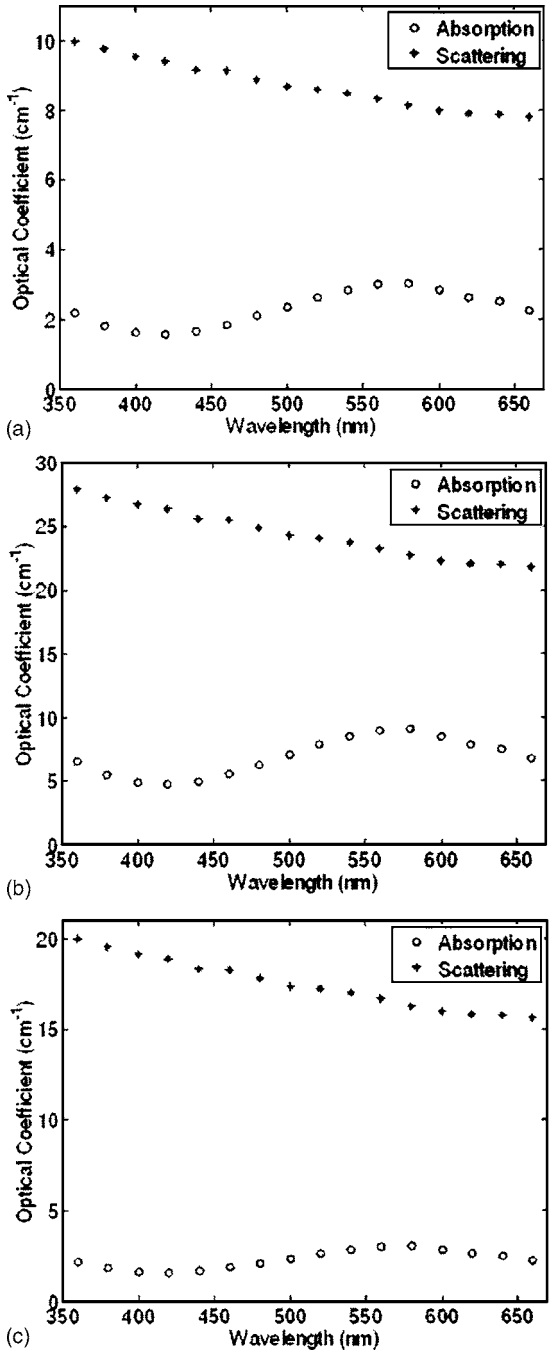

Fig. 3. Absorption and reduced scattering coefficients of the (a) top layer, (b) bottom layer, and (c) middle layer at a range of wavelengths from 360 to 660 nm in a two-layered and a three-layered theoretical epithelial tissue model.

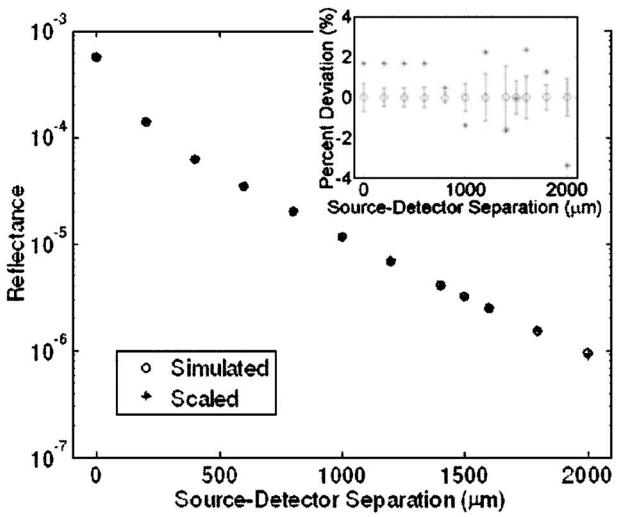

Fig. 4. Diffuse reflectance as a function of the source–detector separation at a single wavelength (500 nm) for the original two-layered epithelial tissue model. The star symbols in the inset are the percent deviations of the scaled reflectance value relative to the mean of six independently simulated reflectance values as calculated in Eq. (1) for each separation. The open circles in the inset represent zero percent deviation. The error bar indicates 95% confidence interval (CI) of the percent deviation of simulated reflectance values relative to its expected value, which was calculated according to Eq. (2).

tance values from six runs of the independent simulation on the same tissue model. The percent deviations of six simulated reflectance values relative to their mean were also calculated in the same manner. The 95% confidence interval (CI) of the percent deviations of simulated reflectance relative to their expected value was then estimated as follows:

$$95\,\%\,\mathrm{CI} = [\mathrm{mean} - 1.96 \times \mathrm{std}/\sqrt{m},\ \mathrm{mean} + 1.96 \times \mathrm{std}/\sqrt{m}], \tag{2}$$

where m is the number of simulation runs ($m=6$) and "mean" and "std" refer to the mean and standard deviation of the calculated percent deviations. It should be pointed out that the mean of the percent deviations is always zero and the 95% CI gives the range of the true percent deviation with a p-value of 0.05.

Figure 4 shows scaled diffuse reflectance and independently simulated diffuse reflectance as a function of source–detector separation at a single wavelength (500 nm) for the original two-layered epithelial tissue model under ideal conditions, where the only source of error besides statistical uncertainty is the scaling operation. The two sets of symbols completely overlap at almost all separations, which indicates excellent agreement between simulated and scaled reflectance values. The inset graph shows the percent deviation of scaled reflectance calculated according to Eq. (1). The 95% CIs of the percent deviations of simulated reflectance relative to their expected value are indicated by the error bars. All the percent deviations of the scaled reflectance are less than 4%; moreover, they are all close to or within the 95% CIs of the percent deviations of simulated reflectance values. On the one hand, small percent deviations of scaled reflectance relative to simulated reflectance are indicative of the validity of the multilayered scaling method. On the other hand, the observation that some data points representing the percent deviations of scaled reflectance are out of the 95% CI of percent deviations of simulated reflectance suggests that the scaling method may contain errors caused by factors other than statistical uncertainty, which will be discussed in Section 4.

Figure 5(a) shows the simulated and scaled diffuse reflectance as a function of wavelength for four representative separations, which are 0, 200, 800, and 1500 μm, and Fig. 5(b) shows the percent deviation between scaled and simulated reflectance as a function of wavelength for the original two-layered epithelial model. It should be pointed out that a separation of 0 μm is the case in which a single fiber is used for both illumination and collection; a separation of 200 μm is the case in which source and detector

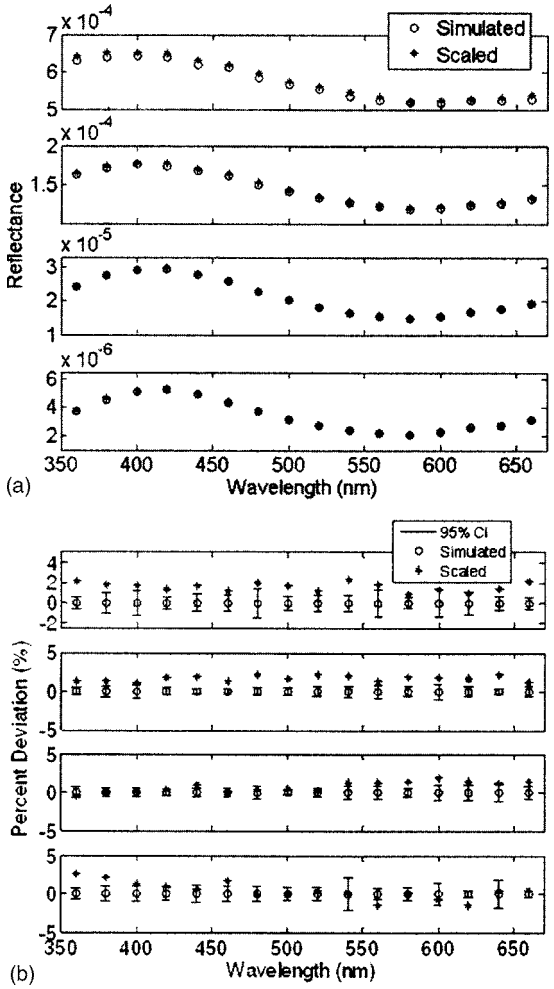

Fig. 5. (a) Simulated and scaled diffuse reflectance and (b) percent deviation of scaled reflectance relative to simulated reflectance [calculated according to Eq. (1)] as a function of wavelength at four separations (0, 200, 800, and 1500 μm in the order from the top to the bottom) for the original two-layered epithelial tissue model. The 95% CI of the percent deviation of simulated reflectance relative to its expected value was calculated according to Eq. (2) and illustrated by the error bars in (b). The open circles in (b) are the mean of the percent deviation of simulated reflectance relative to its expected value, which is always zero because the expected value was estimated by the mean of simulated reflectance.

fibers are placed side by side; a separation of 1500 μm represents a case in which source and detector fibers are placed far away from each other; and a separation of 800 μm is the case in between a small separation (0 μm) and a large separation (1500 μm).

In Fig. 5(a), the line shapes across four separations are similar because there was only one absorber present in the two-layered tissue model. The magnitude of reflectance decreases as the separation increases. The two sets of symbols representing scaled and simulated reflectance overlap completely when the separation is 800 or 1500 μm. The agreement is slightly worse when the separation is 0 or 200 μm.

In Fig. 5(b), the percent deviation of the scaled reflectance relative to the mean of simulated reflectance and 95% CIs of the percent deviation of simulated reflectance from its mean are shown for comparison. The percent deviation between scaled and simulated reflectance is almost always outside of the 95% CI of the percent deviation of simulated reflectance and distributed monotonically on the positive side of the zero-deviation line when the separation is 0 or 200 μm. In contrast, over half of the percent deviations between scaled and simulated reflectance are within the 95% CI of the percent deviation of simulated reflectance and distributed evenly on the positive and negative sides of the zero-deviation line when the separation is 800 or 1500 μm. This finding suggests that the scaling method is better for larger source–detector separations than for smaller separations.

B. Effect of Various Model Parameters on Percent Deviation of Scaled Diffuse Reflectance Relative to Simulated Diffuse Reflectance

Several parameters of the tissue models or probe geometry could affect the valid range of scaled diffuse reflectance when their values are different from those in the baseline simulation. For example, the variation in the anisotropy or refractive index values of the tissue model at different wavelengths can cause a change in diffuse reflectance even when the absorption and scattering coefficients are identical. If the multilayered scaling method, for which only a single set of values can be chosen for those parameters in the baseline simulation, is used to estimate optical properties for a range of wavelengths, such differences in model parameters could cause significant errors in the estimated optical properties. As the first step to evaluate the validity of scaled reflectance, a series of independent Monte Carlo simulations were run for several modified two-layered epithelial tissue models, in each of which one target parameter was varied over a certain range that covers typically seen values, while other parameters in the tissue model and the probe geometry were kept identical to those in the original two-layered epithelial tissue model. Then the differences between scaled reflectance and simulated reflectance were quantitatively evaluated. The root-mean-square error (RMSE) of scaled reflectance relative to independently simulated reflectance calculated over all wavelengths was used to quantify the difference between the simulated and scaled diffuse reflectance, which is defined as follows:

$$\mathrm{RMSE} = \sqrt{\frac{\sum_{i=1}^{n}\left(\frac{\mathrm{Scaled}_i - \mathrm{Simulated}_i}{\mathrm{Simulated}_i} \times 100\right)^2}{n}},$$

where n is the number of wavelengths ($n=16$) and Scaled_i and $\mathrm{Simulated}_i$ correspond to scaled results and simulated results at the ith wavelength, respectively.

1. Anisotropy Factor

Table 1 shows the RMSE of the scaled reflectance values for the original two-layered tissue model where the anisotropy was 0.9, relative to independently simulated reflectance for a modified two-layered epithelial tissue model. The simulated reflectance values for the modified two-layered tissue model were generated for the case where the anisotropy factor of the top layer and bottom layer was varied from 0.7 to 0.8 to 0.9 (this value was used in the baseline simulation) to 0.99 to cover the range of commonly seen anisotropy values in biological tissues.[31] It needs to be pointed out that when the anisotropy was varied in the modified tissue model the scattering coefficient was also changed accordingly to maintain an identical reduced scattering coefficient, in order to test the validity of the first-order similarity relation.[32] All other parameters in the modified and original tissue models remained identical.

For the top layer, it was found that the scaled reflectance for a separation of 0 μm deviates from the simulated reflectance most, which is consistent with the findings from Fig. 5. The RMSEs for a source–detector separation of 0 μm are significantly larger than those for larger separations for anisotropies of 0.7, 0.8, and 0.99. This suggests that the photons collected probably experience many fewer collisions at a separation of 0 μm than at larger separations, thus requiring more precise anisotropy values to obtain accurate diffuse reflectance values. The RMSEs corresponding to $g=0.9$ are always the smallest while those corresponding to $g=0.7$ are always the

Table 1. Effect of Anisotropy Factor of Tissue Layer on RMSE[a]

Variable	RMSE (%) for Separation =0 μm	RMSE (%) for Separation =200 μm	RMSE (%) for Separation =800 μm	RMSE (%) for Separation =1500 μm
Top anisotropy				
$g=0.7$	20.0	4.2	9.5	7.4
$g=0.8$	9.5	1.7	5.1	3.8
$g=0.9$	**1.7**	**1.7**	**1.0**	**1.2**
$g=0.99$	12.3	3.4	3.7	3.6
Bottom anisotropy				
$g=0.7$	0.9	4.1	2.6	2.0
$g=0.8$	0.7	1.3	1.8	1.3
$g=0.9$	**1.7**	**1.7**	**1.0**	**1.2**
$g=0.99$	3.1	3.8	0.8	1.7

[a]RMSEs of scaled reflectance for the original two-layered tissue model relative to independently simulated reflectance for a modified two-layered epithelial tissue model where the anisotropy factor (g) of the top or bottom layer was varied while other parameters of the modified tissue model were kept identical to those of the original tissue model. Note that the anisotropy factor was 0.9 in the original tissue model as shown in bold type.

Table 2. Effect of Refractive Index of Tissue Layer on RMSE[a]

Variable	RMSE (%) for Separation =0 μm	RMSE (%) for Separation =200 μm	RMSE (%) for Separation =800 μm	RMSE (%) for Separation =1500 μm
Top refractive index				
$n=1.3$	2.9	1.6	1.1	1.0
$n=\mathbf{1.338}$	**1.7**	**1.7**	**1.0**	**1.2**
$n=1.4$	8.4	5.8	3.1	3.5
$n=1.5$	17.0	10.2	6.5	6.3
Bottom refractive index				
$n=1.3$	0.9	1.3	3.6	4.7
$n=\mathbf{1.338}$	**1.7**	**1.7**	**1.0**	**1.2**
$n=1.4$	2.5	5.1	8.2	8.1
$n=1.5$	1.2	6.8	20.2	19.6

[a]RMSEs of scaled reflectance for the original two-layered tissue model relative to independently simulated reflectance for a modified two-layered epithelial tissue model where the refractive index of the top or bottom layer was varied while other parameters of the modified two-layered epithelial tissue model were kept identical to those of the original two-layered epithelial tissue model. Note that the refractive index was 1.338 in the original tissue model as shown in bold type.

largest, which implies that the further the anisotropy in an independent test simulation is from the baseline simulation for scaling, the larger the deviation between the scaled and simulated reflectance will be for all source–detector separations. The RMSEs for the bottom layer are generally smaller than those of the top layer for identical anisotropy values, which suggests that the diffuse reflectance is less affected by variation in the anisotropy of the bottom layer. Moreover, there is no clear trend with separation or anisotropy values in the RMSEs of the bottom layer.

2. Refractive Index of the Tissue Layers

Table 2 shows the RMSEs of the scaled reflectance values for the original two-layered epithelial tissue model where the refractive index was 1.338, relative to independently simulated reflectance for a modified two-layered epithelial tissue model where the refractive index of the top layer and the bottom layer was varied from 1.3 to 1.338 (the value used in the baseline simulation for scaling) to 1.4 and to 1.5 to cover the range of commonly seen refractive indices in biological tissues.[33–36] All other parameters in the modified and original tissue models were kept identical.

When the top-layer refractive index was varied, the RMSE decreases in general as the source–detector separation increases. The RMSEs corresponding to $n=1.338$ are always the smallest while those corresponding to $n=1.5$ are always the largest, which suggests that the further the refractive index in an independent test simulation is from that in the baseline simulation, the larger the deviation between the scaled and simulated reflectance will be for all source–detector separations in this study. When the bottom-layer refractive index was varied, the most surprising finding is that the separation of 0 μm was always the best case among all separations in terms of the agreement between scaled and simulated reflectance. The RMSEs for small separations (0 and 200 μm) are generally smaller than those for the other two larger separations (800 and 1500 μm) for all refractive indices that are different from the baseline value. This suggests that the refractive index of the bottom layer does not considerably affect reflectance collected at small separations but can significantly affect reflectance collected at large separations, which is the opposite of the trend in the top layer. Except for a separation of 0 μm, the RMSE increases with the difference between the refractive index of the bottom layer and that in the baseline simulation.

3. Refractive Index of the Medium above the Tissue Model

The medium above the tissue model could be air, water, or synthetic fused silica (the material that glass fibers are usually made of) in a simulation. Figure 6 shows simulated and scaled reflectance as a function of the source–detector separation from a modified two-layered epithelial tissue model at a single wavelength (500 nm), where the refractive index of the medium above the tissue model was varied from 1.0 (air) to 1.338 (water) to 1.462 (synthetic fused silica) and to 1.6 (the upper limit of synthetic fused silica in the UV region).[28] The other parameters were kept identical to those of the original two-layered epithelial tissue model. The symbols corresponding to various refractive indices completely overlap. The inset figure, which gives the percent deviation of scaled reflectance relative to simulated reflectance, confirms that the difference between simulated and scaled reflectance is smaller than 3% except for a separation of 2000 μm. This suggests that the effect of the refractive index of the medium on top of the tissue model on detected diffuse reflectance is negligible compared with other variables that have been studied for separations smaller than 2000 μm. When the separation is equal to or larger than 2000 μm, the small number of photons collected by the detector fi-

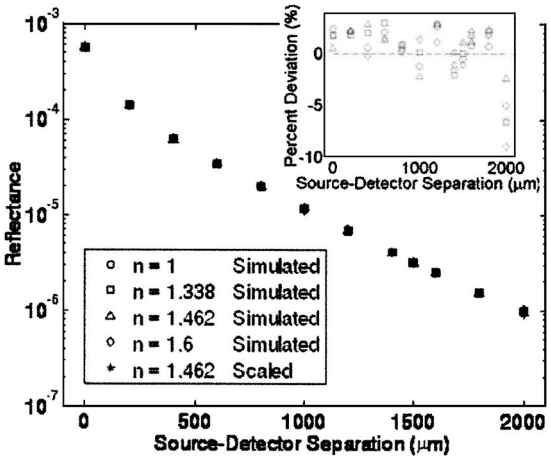

Fig. 6. Simulated reflectance as a function of separation from a modified two-layered epithelial tissue model at a wavelength of 500 nm, where the refractive index of the medium above the tissue model was varied from 1.0 to 1.338 to 1.462 and to 1.6 and other parameters were kept identical to those in the original two-layered epithelial tissue model. The scaled reflectance as a function of separation is also shown, for which the refractive index of the medium above the tissue model was 1.462 in the baseline simulation. The inset graph shows the percent deviation of scaled reflectance relative to simulated reflectance for different refractive indices as a function of separation. The dashed line in the inset represents zero percent deviation.

Table 3. Effect of Refractive Indices of Fiber Core and Tissue Model on Specular Reflectance[a]

n_{fiber} (column)\n_{tissue} (row)	1.3	1.4	1.5
0° incidence			
1.4	0.0014	6.3×10^{-33}	0.0012
1.5	0.0051	0.0012	0
1.6	0.011	0.0044	0.0010
Cutoff angles defined by NA 0.22			
1.4 (θ_{cutoff}=9.0°)	0.0014	7.6×10^{-33}	0.0012
1.5 (θ_{cutoff}=8.4°)	0.0051	0.0012	0
1.6 (θ_{cutoff}=7.9°)	0.011	0.0044	0.0010

[a]Fraction of specular reflectance for various combinations of refractive indices of the fiber core and the tissue model when (top half) the incident angle is 0° and (bottom half) the cutoff angle (θ_{cutoff}) is defined by an NA of 0.22. n_{fiber} represents the refractive index of the fiber core, and n_{tissue} is the refractive index of the tissue model. The actual cutoff angles are also shown in the bottom half of the table.

ber may cause more significant statistical uncertainty, and the effect of the refractive index of the medium above the tissue model could become more important. The same observation can be expected for other wavelengths as long as the optical properties are within a similar range.

4. Refractive Index of the Fiber Core

The refractive index of the fiber core could be another unknown in the simulation, which varies with wavelength but may not be conveniently measured. Considering that source and detector fiber tips usually occupy only a small area on the top surface of the tissue, the effect of the fiber core on those photons that hit the fiber core area and are then reflected back into the tissue will be assumed to be negligible during photon propagation in the tissue model. Therefore, the problem will be simplified by considering only photon launch from the source fiber end and photon collection on the detector fiber end. On the source end, the change in the refractive index of a fiber core can cause variations in the fraction of specular reflectance. Table 3 lists the specular reflectance values calculated according to Fresnel's equation for (top half) 0° incidence and (bottom half) cutoff angles defined by an NA of 0.22 for various combinations of refractive indices of the fiber core (commonly seen refractive index values of synthetic fused silica[28] in the UV-VIS spectral region) and the tissue model. It can be seen that the change in specular reflectance is negligible when the incident angle is varied from 0° to the cutoff angle defined by an NA of 0.22. In Table 3, the greatest specular reflectance occurs when n_{fiber}=1.6 and n_{tissue}=1.3, in which case the specular reflectance is around 1%, and this percentage is comparable with the percent variation in diffuse reflectance due to statistical uncertainty shown in Fig. 4. This small specular reflectance suggests that the variations in the refractive index of the fiber core do not cause significant variation in the amount of light delivered into the tissue model for an NA equal to or smaller than 0.22.

On the detector end, the cutoff acceptance angle defined by an NA can be calculated by $\arcsin(NA/n_{tissue})$, where n_{tissue} refers to the refractive index of the tissue model, which is independent of the refractive index of the fiber core if the NA is fixed. Therefore the refractive index of the fiber core has no impact on photon collection for a fixed NA.

5. Phase Function

The Henyey–Greenstein (HG) phase function and the Mie phase function are commonly used in Monte Carlo simulations of light transport in tissue. Figure 7 shows the diffuse reflectance simulated for the Mie phase function used in both layers (calculated by Mie theory[30] for the polystyrene spheres in the theoretical phantom as in Subsection 2.C at 500 nm), the diffuse reflectance simulated for the HG phase function with an anisotropy factor of 0.93 (equal to that of the Mie phase function) used in both layers, and the scaled reflectance for the original two-layered epithelial tissue model (the anisotropy factor was fixed at 0.9). This graph demonstrates that the diffuse reflectance simulated with the Mie phase function is significantly different from that simulated with the HG phase function as well as from the scaled diffuse reflectance, especially for a separation of 0 μm (see the inset graph). As the separation becomes larger, the percent deviation between the scaled reflectance and the diffuse reflectance simulated with the Mie phase function fluctuates and asymptotically approaches a small value, which implies that the first-order similarity relation holds for large separations. In contrast, the percent deviation between the scaled reflectance and the diffuse reflectance simulated with the HG phase function always oscillates around zero.

Table 4 shows the RMSEs between scaled and simulated (HG versus Mie) reflectance for all 16 wavelengths for four representative separations. The diffuse reflectance simulated with the Mie phase function demonstrates considerably larger deviation compared with that simulated with the HG phase function for all separations, which suggests that the choice of the phase function is

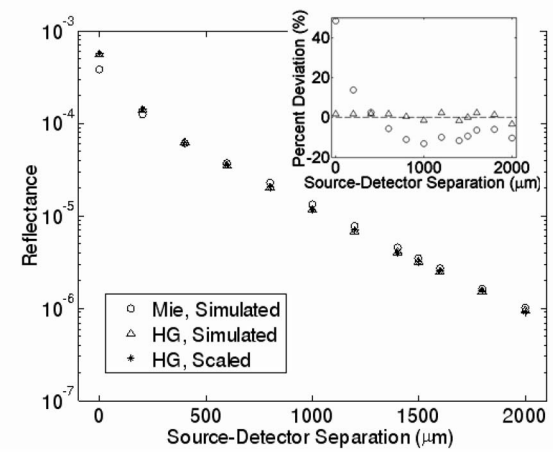

Fig. 7. Simulated reflectance as a function of separation at a wavelength of 500 nm for a modified two-layered epithelial tissue model, in which the phase function was calculated from Mie theory[30] and other parameters including absorption and reduced scattering coefficients were kept identical to the original two-layered epithelial tissue model. The reflectance simulated for the original two-layered epithelial tissue model and the scaled reflectance, in which the HG phase function was used, are also shown for comparison. The inset graph shows the percent deviation of scaled reflectance relative to the two sets of simulated reflectance. The dashed line in the inset represents zero deviation.

Table 4. Effect of Phase Function on RMSE[a]

Variable	RMSE (%) for Separation =0 μm	RMSE (%) for Separation =200 μm	RMSE (%) for Separation =800 μm	RMSE (%) for Separation =1500 μm
HG	1.7	1.7	1.0	1.2
Mie	40.0	13.5	10.1	9.3

[a]RMSEs of scaled reflectance relative to independently simulated reflectance from a modified two-layered epithelial tissue model in the case that the phase function was changed from the HG function to the Mie function while other parameters of the modified two-layered epithelial tissue model were kept identical to those of the original two-layered epithelial tissue model. Note that the HG phase function was used in the baseline simulation for scaling.

Table 5. Effect of One Additional Layer and Layer Thickness on RMSE[a]

Variable	RMSE (%) for Separation =0 μm	RMSE (%) for Separation =200 μm	RMSE (%) for Separation =800 μm	RMSE (%) for Separation =1500 μm
Top-layer thickness (μm)				
d_3=50	1.1	0.4	0.6	1.3
d_3=250	1.7	1.4	0.5	2.8
d_3=450	2.2	1.2	0.7	1.2

[a]RMSEs of scaled reflectance relative to corresponding independently simulated reflectance for a three-layered epithelial tissue model, whose structure and optical properties were, respectively, shown in Figs. 2(b) and 3. While the thickness of the top layer (d_3) was varied from 50 to 250 and to 450 μm, the thickness of the middle layer was changed from 450 to 250 and to 50 μm accordingly to keep the total thickness of the two layers a constant (500 μm). The anisotropy factor and refractive index of each layer as well as the choice of the phase function (HG) in the tissue model were identical to those in the baseline simulation for scaling.

critical when diffuse reflectance in the UV-VIS spectral region for small source–detector separations is quantitatively modeled.

C. Effect of Three Layers and Layer Thickness on Percent Deviation of Scaled Diffuse Reflectance Relative to Simulated Diffuse Reflectance

The RMSEs of scaled reflectance relative to corresponding independently simulated reflectance for a three-layered tissue model with the top layer at various thicknesses, whose structure and optical properties are shown, respectively, in Figs. 2(b) and 3, are listed in Table 5. It should be noted that the only difference between the three-layered tissue model and the baseline simulation for scaling is the number of layers and optical properties. The purpose of this comparison is not only to test the validity of the multilayered scaling method for a tissue model with more layers but also to test whether a layer as thin as 50 μm in the tissue model, which is comparable with the smallest depth interval width and the mean transport free path in the baseline simulation, would cause a significant deviation between scaled and simulated reflectance.

It is observed that the RMSEs shown in Table 5 for the three-layered tissue model are generally comparable to those shown in Table 1 for the original two-layered tissue model with g=0.9. Additionally, the RMSEs for the three-layered tissue model with a 50 μm thick layer (when d_3 =50 or 450 μm) are comparable to the RMSEs for the three-layered tissue model with the thickness of all layers significantly greater than 50 μm (when d_3=250 μm), which implies that a layer in a multilayered tissue model whose thickness is comparable to the smallest depth interval width and/or the mean transport free path in the baseline simulation for scaling does not cause the deviation between scaled diffuse reflectance and corresponding simulated reflectance to be considerably larger than thicker layers.

D. Effect of Anisotropy Factors, Refractive Indices, and Phase Functions on the Accuracy of Optical Property Estimation Using the Monte Carlo Reflectance Database Obtained with the Multilayered Scaling Method

The purpose of this part of the study was to examine how the deviations in the scaled diffuse reflectance relative to the independently simulated reflectance shown in Tables 1, 2, and 4 are propagated as errors in estimating the optical properties of a multilayered medium. As described previously,[16] our group has developed an approach called the sequential estimation approach to estimate the optical properties of a two-layered epithelial tissue-like medium. The optical properties of the first layer are determined from diffuse reflectance spectra obtained with a specialized angled probe geometry using a scalable Monte Carlo model[21] for a homogeneous medium. Then a second Monte Carlo model is employed to estimate the bottom-layer optical properties and the top-layer thickness from diffuse reflectance spectra obtained with a standard flat-tip fiber-optic probe geometry. In the previous publication, a database that contains diffuse reflectance data obtained by running multiple independent simulations from the two-layered tissue model for a wide range of optical properties was required prior to the inversion process to estimate the optical properties for the bottom layer. In the simulation study described in this paper, the computationally intensive process of running multiple independent simulations is replaced by using the multilayered scaling method. In the process of implementing the inversion, the optical properties of the top layer are assumed as known. The deviation between estimated and true optical properties for the wavelength range of interest was represented by the RMSE.

Tables 6–8 list the RMSEs of estimated optical properties of the bottom layer and thickness of the top layer relative to the corresponding true values for given simulated diffuse reflectance spectra at a source–detector separation of 1500 μm from the same modified two-layered epithelial tissue models used in Tables 1, 2, and 4. It can be seen in Tables 6–8 that the RMSEs in the case where the anisotropies, refractive indices, and the phase functions of the two-layered tissue model are identical to those used in the baseline simulation are comparable with those obtained previously using a Monte Carlo database created with independently simulated data[16] for the same two-layered tissue model and probe geometry. Other results will be discussed in the next section for conciseness.

4. DISCUSSION

A multilayered scaling method has been developed to quickly calculate diffuse reflectance for a wide range of optical properties based on a single baseline Monte Carlo simulation. For example, a single Monte Carlo simulation with 10^7 incident photons for the two-layered tissue model shown in Fig. 2(a) took 1–2 h in a Sun Unix workstation with a 1 GHz UltraSPARC-IIIi CPU and 1 GByte RAM when the HG phase function was used. The baseline simulation for scaling in this study was run with 4×10^6 incident photons, which took about 35 h on the same type of computer. After the photon trajectory information was obtained from the baseline simulation, it took about 4 s to scale for the two-layered tissue model and 5 s for the three-layered tissue model shown in Fig. 2. The multilayered scaling method reduces the computation time by more than 2 orders of magnitude compared with independent Monte Carlo simulations. The multilayered scaling method could be further optimized, for example by applying parallel computation, to achieve even faster computation than reported here. The multilayered scaling method can also be easily extended to more complicated probe geometries, for example, a probe geometry with oblique illumination and collection.[16,37] Requiring only one baseline simulation makes this method particularly suited to simulating diffuse reflectance spectra in a multilayered medium for a wide range of optical properties and for a variety of different probe geometries and/or creating a Monte Carlo database for estimating optical properties of layered media, which can potentially help increase the use of Monte Carlo modeling in spectroscopy research of layered tissues.

The scaling relations used in this study could also play a role in simplifying phantom fabrication. Figure 8(a) shows a flat-tip fiber-optic probe geometry for diffuse reflectance measurement from a semi-infinite two-layered epithelial tissue phantom, and Fig. 8(b) shows the scaled version of the phantom and the probe geometry. The physical dimensions of both the phantom and the fiber-optic probe are scaled up by a factor of N while the transport coefficients of the phantom are scaled down by the same factor in the scaled version. It is straightforward to see that the diffuse reflectance measured in Figs. 8(a) and 8(b) would be identical as can be inferred from the two representative scaled trajectories, which has also been confirmed by actual diffuse reflectance calculation for the two phantoms using the multilayered scaling method (results not shown). One example of applications for the scaled phantom is to replace a phantom whose top-layer thickness d_1 is very small with a scaled phantom whose top layer is much thicker. By scaling up the dimensions of the phantom and the probe as shown in Fig. 8(b), identical diffuse reflectance can be measured from the scaled phantom in which the thickness of the top layer is N times the original thickness and thus easier to make. Similar ideas can be used to scale other parameters to make them easier to achieve when the phantom with raw parameters is not feasible to fabricate. It should be noted

Table 6. Effect of Anisotropy Factor of Tissue Layer on RMSE of Estimated Optical Properties[a]

Variable	Thickness of Top Layer	μ_{a_bottom}	μ'_{s_bottom}	RMSE (%) >20%?
Top anisotropy				
$g=0.7$	−12.7	10.5	45.2	Y
$g=0.8$	−11.5	9.6	15.5	
$g=0.9$	**9.6**	**9.5**	**5.9**	
$g=0.99$	−6.2	10.5	8.4	
Bottom anisotropy				
$g=0.7$	−9.0	8.3	12.8	
$g=0.8$	−26.6	21.3	7.7	Y
$g=0.9$	**9.6**	**9.5**	**5.9**	
$g=0.99$	−10.2	12.1	6.5	

[a]RMSEs of the estimated thickness of the top layer and optical properties of the bottom layer relative to the corresponding true values for given sets of simulated diffuse reflectance spectra from the same modified two-layered epithelial tissue models as in Table 1, where the anisotropy factor of the top or bottom layer was varied while other parameters in the modified two-layered epithelial tissue models were kept identical to those in the original two-layered epithelial tissue model. The rows with bold type are the RMSEs of estimated parameters for input diffuse reflectance simulated with exactly the same anisotropy factor as in the baseline simulation for scaling. The rightmost column in the table indicates if a row contains an RMSE greater than 20% (marked by "Y"), which is a sign of inaccurate inversion.

Table 7. Effect of Refractive Index of Tissue Layer on RMSE of Estimated Optical Properties[a]

Variable	Thickness of Top Layer	μ_{a_bottom}	μ'_{s_bottom}	RMSE (%) >20%?
Top refractive index				
$n=1.3$	6.3	2.1	25.0	Y
$n=1.338$	**9.6**	**9.5**	**5.9**	
$n=1.4$	−7.5	7.8	45.4	Y
$n=1.5$	−7.1	7.1	76.3	Y
Bottom refractive index				
$n=1.3$	4.2	1.4	28.8	Y
$n=1.338$	**9.6**	**9.5**	**5.9**	
$n=1.4$	−14.5	6.9	2.5	
$n=1.5$	−11.6	6.0	14.3	

[a]RMSEs of the estimated thickness of the top layer and optical properties of the bottom layer relative to the corresponding true values for given sets of simulated diffuse reflectance spectra from the same modified two-layered epithelial tissue models as in Table 2, where the refractive index of the top or bottom layer was varied while other parameters in the modified two-layered epithelial tissue models were kept identical to those in the original two-layered epithelial tissue model. The rows with bold type are the RMSEs of estimated parameters for input diffuse reflectance simulated with exactly the same refractive index as in the baseline simulation for scaling. The rightmost column in the table indicates if a row contains an RMSE greater than 20% (marked by "Y"), which is a sign of inaccurate inversion.

Table 8. Effect of Phase Function on RMSE of Estimated Optical Properties[a]

Variable	Thickness of Top Layer	μ_{a_bottom}	μ'_{s_bottom}	RMSE (%) >20%?
HG	**9.6**	**9.5**	**5.9**	
Mie	−30	31.4	5.0	Y

[a]RMSEs of the estimated thickness of the top layer and optical properties of the bottom layer relative to the corresponding true values for given sets of simulated diffuse reflectance spectra from the same modified two-layered epithelial tissue models as in Table 4, where the phase function was changed from the HG function to the Mie function while other parameters in the modified two-layered epithelial tissue models were kept identical to those in the original two-layered epithelial tissue model. The rows with bold type are the RMSEs of estimated parameters for input diffuse reflectance simulated with exactly the same phase function as in the baseline simulation for scaling. The rightmost column in the table indicates if a row contains an RMSE greater than 20% (marked by "Y"), which is a sign of inaccurate inversion.

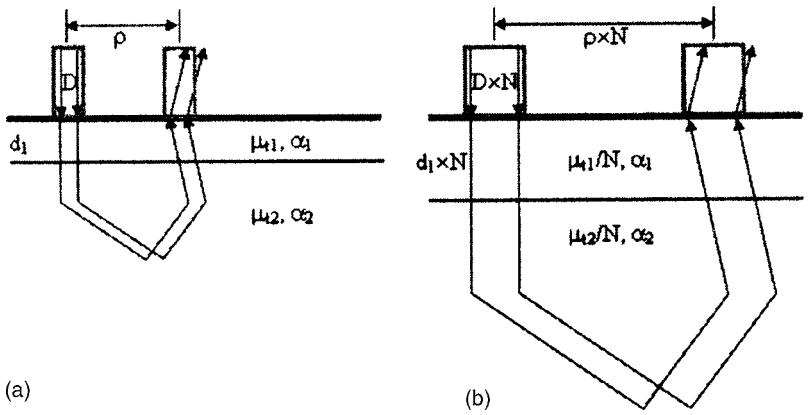

Fig. 8. (a) Schematic of a flat-tip fiber-optic probe geometry for diffuse reflectance measurement from a semi-infinite two-layered epithelial tissue phantom and (b) the scaled version of the phantom and the probe geometry. In (a), μ_{t1} and μ_{t2} are the transport coefficients of the top and bottom layers, α_1 and α_2 are the albedos of the two layers, the thickness of the top layer is d_1, the diameter of both source and detector fibers is D, and the source–detector separation is ρ. In (b), the transport coefficients of the top and bottom layers are μ_{t1}/N and μ_{t2}/N, the albedos of the two layers are still α_1 and α_2, the thickness of the top layer becomes $d_1 \times N$, the diameter of both source and detector fibers is $D \times N$, and the source–detector separation is $\rho \times N$. Two representative photon trajectories were drawn in both (a) and (b) to illustrate the scaling operation.

that when the same scatterer is used in the raw phantom and in the scaled phantom, the variation in the dimension of the phantom and the probe could cause a change in the validity of a simplified phase function, e.g., using the HG phase function with an identical anisotropy factor to replace the Mie phase function is not accurate for small source–detector separations but is accurate for large separations.

Although the difference between scaled and simulated reflectance is small under ideal conditions as shown in Figs. 4 and 5, the Fig. 4 inset and Fig. 5(b) demonstrate that scaled reflectance is slightly out of the 95% CI of simulated reflectance that is determined by the statistical uncertainty. Besides the difference in the number of incident photons between test simulations and the baseline simulation for scaling, the main reason for this observation is that the photon trajectory information can only be recorded in several depth intervals with finite widths. When the layer interface in a two-layered tissue model was mapped to the baseline homogeneous model for scaling, the interface would fall either exactly at a boundary between two adjacent depth intervals or within a depth interval. In the former case, the scaling result would be identical to the simulated result from an equivalent independent Monte Carlo simulation. However, a systematic error would be induced in the latter case because the offset and number of collisions in this depth interval are distributed between the two relevant pseudolayers and the contribution to each layer is proportional to the fraction of the interval width within that layer. This step inherently assumes that the offset and number of all collisions are uniformly distributed within a depth interval, which is not always true in an independent simulation. A scheme that records the photon density as a function of depth at a finer resolution to more precisely determine this distribution could improve the accuracy. Alternatively, smaller depth interval widths in the most populated region of photon visitation could be chosen to reduce this error. As a rule of thumb, an interval width that is comparable to the mean transport free path in the baseline simulation for the depth within 1000 μm would yield an acceptable systematic error as demonstrated in Figs. 4 and 5. Given that finer depth intervals require more memory space to store the photon trajectory information, a scheme of variable depth interval widths used in this study (refer to Subsection 2.B for details) can be used as a trade-off. In addition, certain variance reduction techniques, such as geometry splitting,[16,17] can be used to increase the number of useful photons in scaling, thus reducing the statistical uncertainty of scaled results when a narrow range of optical properties and source–detector separations are evaluated.

Tables 1, 2, and 4 show the RMSEs of scaled reflectance relative to independently simulated reflectance in the case where one model parameter was changed at a time. It can be seen that the RMSE value could vary over a large range depending on which parameter is changed. The validity of scaled results depends upon the accuracy requirement of specific applications when the target layered tissue model contains parameters whose values are not equal to the baseline ones. For example, if one needs to see only the general trend of forward diffuse reflectance spectra for a certain fiber-optic geometry, perhaps a RMSE of 10% will be tolerable. However, if the multilayered scaling result is used to create a Monte Carlo database for inversion to estimate optical properties, a smaller RMSE may be required. For a two-layered epithelial tissue model in general,

(1) Diffuse reflectance is more sensitive to the anisotropy factor of the top layer than to the anisotropy of the bottom layer when the HG phase function is used in the baseline simulations. This may be attributed to the fact that photons are multiply scattered before they reach the bottom layer. Moreover, the diffuse reflectance obtained at a small separation (0 μm) is more sensitive to the anisotropy factor of the top layer than those measured at larger separations (200, 800, and 1500 μm) for a similar reason;

i.e., photons have been multiply scattered upon detection for larger separations. Similar trends are not observed for the bottom layer.

(2) Diffuse reflectance simulated for small source–detector separations (0 and 200 μm) is more sensitive to the refractive index of the top layer while diffuse reflectance simulated for large separations (800 and 1500 μm) is more sensitive to the refractive index of the bottom layer, which can be explained as follows.

When the refractive index of the top layer changes, refractive index mismatch occurs at both the interface between the medium above the tissue model and the top layer and the interface between the top and bottom layers. The photons detected for small source–detector separations primarily travel in the top layer so the diffuse reflectance collected for small separations is primarily influenced by the refractive index mismatch between the top layer and the medium above it. When the refractive index of the bottom layer changes, the diffuse reflectance collected for small separations will be influenced only minimally because the detected photons primarily travel in the top layer. However, the diffuse reflectance collected at the larger separations will be influenced more significantly by the refractive index of the bottom layer because the detected photons are more likely to travel within this part of the tissue.

(3) Diffuse reflectance for all source–detector separations in this study (0, 200, 800, 1500 μm) is sensitive to the choice of the phase function. For applications that require high accuracy in diffuse reflectance, such as precise estimation of optical properties in layered media, the high-order moments of the phase function need to be considered for these separations.[12,38]

In the study of using the multilayered scaling method for inversion (Subsection 3.D), it is found to be difficult to correlate the RMSEs in diffuse reflectance as shown in Tables 1, 2, and 4 with the RMSEs in estimated parameters as shown in Tables 6–8 presumably because of the interplay among three free parameters and the statistical uncertainty of simulated results. For example, while Table 1 demonstrates that the anisotropy factor in the bottom layer has a smaller effect on diffuse reflectance than that in the top layer does, the RMSEs in estimated optical properties in Table 6 do not necessarily agree with that if all three free parameters were considered simultaneously. It is also found that, when the number of free parameters was reduced from three to two and then to one, the RMSEs of estimated parameters become much smaller and the correlation between the RMSE of forward diffuse reflectance and that of estimated parameters improves progressively (results not shown due to limited space). Another important finding is that the RMSEs in estimated parameters are in general considerably larger than those in forward diffuse reflectance. For example, when the anisotropy factor is 0.8 in the bottom layer, the RMSE of the forward diffuse reflectance for the separation of 1500 μm is 1.3% in Table 1, which is comparable to the RMSEs of diffuse reflectance for $g=0.9$ and $g=0.99$. In contrast, the RMSEs of estimated optical properties for $g=0.8$ are considerably larger than those for $g=0.9$ and $g=0.99$ in Table 6. This special case suggests that a small deviation in the forward reflectance due to the change in one parameter of the tissue model could result in a much larger error in estimated optical properties. This observation highlights the need of accurate light transport modeling for the estimation of optical properties in the UV-VIS region for source–detector separations smaller than 2000 μm when there are several free parameters but only limited data.

Because a scaled result is obtained by applying the scaling operation to the photon trajectory data generated by the baseline Monte Carlo simulation, its accuracy depends on both the scaling operation and the baseline Monte Carlo simulation. The errors induced by the two sources seem to be independent of each other. Thus, the convergence of the proposed method depends primarily on the number of detected photons, i.e., the standard deviation of diffuse reflectance is proportional to the square root of number of detected photons. Although our study has shown that the multilayered scaling method works for a layered tissue model with layer thicknesses as thin as one half of the mean transport free path and source–detector separations as large as 40 mean transport free paths, the validity of the method for a specific problem should be empirically evaluated (for example, in the near-infrared wavelength range where the source–detector separations are significantly greater than those presented in this paper).

5. CONCLUSIONS

A multilayered scaling method has been developed to calculate diffuse reflectance for a wide range of optical properties based on the photon trajectory information generated from a single baseline Monte Carlo simulation, which can dramatically reduce the computation time of using Monte Carlo modeling for spectroscopy studies of layered media. This method was tested on both two-layered and three-layered epithelial tissue models. The deviation between scaled diffuse reflectance and independently simulated diffuse reflectance was comparable to the statistical variation between simulated diffuse reflectances from repeated independent simulations. Moreover, the scaling method was used to create a Monte Carlo database for a two-layered tissue model. The database was then employed to estimate the optical properties of the bottom layer and the thickness of the top layer for given simulated diffuse reflectance spectra from the two-layered epithelial tissue model. It was found that the accuracy of estimated parameters was comparable to that achieved previously using another Monte Carlo database that was constructed with independently simulated Monte Carlo data. The scaling method is particularly suited to simulating diffuse reflectance spectra or creating a Monte Carlo database to estimate optical properties of layered media, which can potentially help expand the use of Monte Carlo modeling in the spectroscopy studies of layered tissues.

ACKNOWLEDGMENTS

The authors appreciate helpful discussions with Greg Palmer on this work. This research was supported by the National Institutes of Health grant R21 CA108490.

Corresponding author N. Ramanujam can be reached by phone, 919-660-5307; fax, 919-684-4488; or e-mail, nimmi@duke.edu.

REFERENCES

1. G. M. Palmer, C. Zhu, T. M. Breslin, F. Xu, K. W. Gilchrist, and N. Ramanujam, "Monte Carlo-based inverse model for calculating tissue optical properties. Part II: Application to breast cancer diagnosis," Appl. Opt. **45**, 1072–1078 (2006).
2. W. Verkruysse, R. Zhang, B. Choi, G. Lucassen, L. O. Svaasand, and J. S. Nelson, "A library based fitting method for visual reflectance spectroscopy of human skin," Phys. Med. Biol. **50**, 57–70 (2005).
3. S. Merritt, F. Bevilacqua, A. J. Durkin, D. J. Cuccia, R. Lanning, B. J. Tromberg, G. Gulsen, H. Yu, J. Wang, and O. Nalcioglu, "Coregistration of diffuse optical spectroscopy and magnetic resonance imaging in a rat tumor model," Appl. Opt. **42**, 2951–2959 (2003).
4. R. M. P. Doornbos, R. Lang, M. C. Aalders, F. W. Cross, and H. J. C. M. Sterenborg, "The determination of *in vivo* human tissue optical properties and absolute chromophore concentrations using spatially resolved steady-state diffuse reflectance spectroscopy," Phys. Med. Biol. **44**, 967–981 (1999).
5. G. Zonios, L. T. Perelman, V. Backman, R. Manoharan, M. Fitzmaurice, J. Van Dam, and M. S. Feld, "Diffuse reflectance spectroscopy of human adenomatous colon polyps *in vivo*," Appl. Opt. **38**, 6628–6637 (1999).
6. I. Pavlova, K. Sokolov, R. Drezek, A. Malpica, M. Follen, and R. Richards-Kortum, "Microanatomical and biochemical origins of normal and precancerous cervical autofluorescence using laser-scanning fluorescence confocal microscopy," Photochem. Photobiol. **77**, 550–555 (2003).
7. T. Collier, D. Arifler, A. Malpica, M. Follen, and R. Richards-Kortum, "Determination of epithelial tissue scattering coefficient using confocal microscopy," IEEE J. Sel. Top. Quantum Electron. **9**, 307–313 (2003).
8. R. Drezek, C. Brookner, I. Pavlova, I. Boiko, A. Malpica, R. Lotan, M. Follen, and R. Richards-Kortum, "Autofluorescence microscopy of fresh cervical-tissue sections reveals alterations in tissue biochemistry with dysplasia," Photochem. Photobiol. **73**, 636–641 (2001).
9. N. Ramanujam, R. Richards-Kortum, S. Thomsen, A. Mahadevan-Jansen, and M. Follen, "Low temperature fluorescence imaging of freeze-trapped human cervical tissues," Opt. Express **8**, 335–343 (2000).
10. R. L. P. van Veen, H. J. C. M. Sterenborg, A. Pifferi, A. Torricelli, E. Chikoidze, and R. Cubeddu, "Determination of visible near-IR absorption coefficients of mammalian fat using time- and spatially resolved diffuse reflectance and transmission spectroscopy," J. Biomed. Opt. **10**, 54004 (2005).
11. T. J. Farrell, M. S. Patterson, and B. Wilson, "A diffusion theory model of spatially resolved, steady-state diffuse reflectance for the noninvasive determination of tissue optical properties *in vivo*," Med. Phys. **19**, 879–888 (1992).
12. F. Bevilacqua, D. Piguet, P. Marquet, J. D. Gross, B. J. Tromberg, and C. Depeursinge, "*In vivo* local determination of tissue optical properties: applications to human brain," Appl. Opt. **38**, 4939–4950 (1999).
13. A. Kienle, L. Lilge, M. S. Patterson, R. Hibst, R. Steiner, and B. C. Wilson, "Spatially resolved absolute diffuse reflectance measurements for noninvasive determination of the optical scattering and absorption coefficients of biological tissue," Appl. Opt. **35**, 2304–2314 (1996).
14. A. Kienle and M. S. Patterson, "Determination of the optical properties of turbid media from a single Monte Carlo simulation," Phys. Med. Biol. **41**, 2221–2227 (1996).
15. C. K. Hayakawa, T. Spanier, F. Bevilacqua, A. K. Dunn, J. S. You, B. J. Tromberg, and V. Venugopalan, "Perturbation Monte Carlo methods to solve inverse photon migration problems in heterogeneous tissues," Opt. Lett. **26**, 1335–1337 (2001).
16. Q. Liu and N. Ramanujam, "Sequential estimation of optical properties of a two-layered epithelial tissue model from depth-resolved ultraviolet–visible diffuse reflectance spectra," Appl. Opt. **45**, 4776–4790 (2006).
17. X-5 Monte Carlo Team, "MCNP Vol. I: Overview and Theory," http://mcnp-green.lanl.gov/manual.html (Diagnostics Applications Group, Los Alamos National Laboratory, 2003), pp. 130–158.
18. E. Tinet, S. Avrillier, and J. M. Tualle, "Fast semianalytical Monte Carlo simulation for time-resolved light propagation in turbid media," J. Opt. Soc. Am. A **13**, 1903–1915 (1996).
19. E. Battistelli, P. Bruscaglioni, A. Ismaelli, and G. Zaccanti, "Use of two scaling relations in the study of multiple-scattering effects on the transmittance of light beams through a turbid atmosphere," J. Opt. Soc. Am. A **2**, 903–911 (1985).
20. R. Graaff, M. Koelink, F. de Mul, W. Zijlstra, and A. C. M. Dassel, "Condensed Monte Carlo simulations for the description of light transport," Appl. Opt. **32**, 426–434 (1993).
21. G. M. Palmer and N. Ramanujam, "Monte Carlo-based inverse model for calculating tissue optical properties. Part I: Theory and validation on synthetic phantoms," Appl. Opt. **45**, 1062–1071 (2006).
22. A. Sassaroli, C. Blumetti, F. Martelli, L. Alianelli, D. Contini, A. Ismaelli, and G. Zaccanti, "Monte Carlo procedure for investigating light propagation and imaging of highly scattering media," Appl. Opt. **37**, 7392–7400 (1998).
23. J. Swartling, A. Pifferi, A. M. K. Enejder, and S. Andersson-Engels, "Accelerated Monte Carlo models to simulate fluorescence spectra from layered tissues," J. Opt. Soc. Am. A **20**, 714–727 (2003).
24. The Condor Team, "Condor—high throughput computing," http://www.cs.wisc.edu/condor/ (1997–2006).
25. L. Wang, S. L. Jacques, and L. Zheng, "MCML—Monte Carlo modeling of light transport in multi-layered tissues," Comput. Methods Programs Biomed. **47**, 131–146 (1995).
26. Q. Liu, C. Zhu, and N. Ramanujam, "Experimental validation of Monte Carlo modeling of fluorescence in tissues in the UV–visible spectrum," J. Biomed. Opt. **8**, 223–236 (2003).
27. P. Laven, "Refractive index of water as a function of wavelength," http://www.philiplaven.com/p20.html (2003).
28. I. H. Malittson, "Refractive index versus wavelength reference table measured at 20 °C: synthetic fused silica," http://www.polymicro.com/catalog/a_12.htm (1965).
29. R. Drezek, K. Sokolov, U. Utzinger, I. Boiko, A. Malpica, M. Follen, and R. Richards-Kortum, "Understanding the contributions of NADH and collagen to cervical tissue fluorescence spectra: modeling, measurements, and implications," J. Biomed. Opt. **6**, 385–396 (2001).
30. F. C. Bohren and R. D. Huffman, *Absorption and Scattering of Light by Small Particles* (Wiley, 1983).
31. W.-F. Cheong, "Appendix to Chapter 8: summary of optical properties," in *Optical-Thermal Response of Laser-Irradiated Tissue*, A. J. Welch and M. J. C. van Gemert, eds. (Plenum, 1995), pp. 275–303.
32. D. R. Wyman, M. S. Patterson, and B. C. Wilson, "Similarity relations for anisotropic scattering in Monte Carlo simulations of deeply penetrating neutral particles," J. Comput. Phys. **81**, 137–150 (1989).
33. J. J. J. Dirckx, L. C. Kuypers, and W. F. Decraemer, "Refractive index of tissue measured with confocal microscopy," J. Biomed. Opt. **10**, 44014 (2005).
34. L. Jiancheng, L. Zhenhua, W. Chunyong, and H. Anzhi, "Experimental measurement of the refractive index of biological tissues by total internal reflection," Appl. Opt. **44**, 1845–1849 (2005).

35. V. Tsenova and E. V. Stoykova, "Refractive index measurement in human tissue samples," in Proc. SPIE **5226**, 413–417 (2003).
36. G. J. Tearney, M. E. Brezinski, J. F. Southern, B. E. Bouma, M. R. Hee, and J. G. Fujimoto, "Determination of the refractive index of highly scattering human tissue by optical coherence tomography," Opt. Lett. **20**, 2258–2260 (1995).
37. Q. Liu and N. Ramanujam, "Experimental proof of the feasibility of using an angled fiber-optic probe for depth-sensitive fluorescence spectroscopy of turbid media," Opt. Lett. **29**, 2034–2036 (2004).
38. F. Bevilacqua and C. Depeursinge, "Monte Carlo study of diffuse reflectance at source–detector separations close to one transport mean free path," J. Opt. Soc. Am. A **16**, 2935–2945 (1999).